Research on Cavitation Effect of Microtextured Array

Yuanyuan Jiang
Dalian Maritime University
Zhijun Yan (yanzj@dlmu.cn)
Dalian Maritime University
Shengwei Zhang
Dalian Maritime University
Haocheng Sun
Dalian Maritime University
Ziyu Shen
Dalian Maritime University

Article

Keywords: Micro-textured array, Hydrodynamic lubrication, Morphological characteristics, Cavitation

Posted Date: April 21st, 2022

DOI: https://doi.org/10.21203/rs.3.rs-1567760/v1

Abstract

In this paper, the surface texture parameters and distribution patterns are studied by numerical simulation and experiment. First, a three-dimensional micro-textured CFD fluid lubrication model with cavitation effect is established, and different texture arrays are designed to study the influence of different distribution modes on bearing capacity, friction coefficient and pressure distribution of the oil film. Then, the simulation results are further analyzed and verified by the visualized plane slider experimental platform, and the formation rules of cavitation bubbles in the micro-textured array, as well as the influences of the surface shape and different distribution modes of the micro-textured array on the cavitation bubbles are discussed. The results show that the existence of cavitation is one of the main reasons for the microtexture to increase the bearing capacity of the oil film, which cannot be ignored in the simulation study. The texture array with single symmetric orientation is the best to improve the oil film bearing capacity, and the bearing performance is the best when the texture inclination angle is 26.6°.The friction coefficient of the asymmetrically oriented textured array is 29.4% lower than that of the non-textured sample.The results in the experiment are consistent with the simulation.

1 Introduction

Surface texturing,which generally use a specific processing technology to prepare the microstructure with a certain size, shape and arrangement on the surface of the friction pair, can be applied to improve the hydrodynamic lubrication performance of mechanical components [1]. Surface texture with a reasonable design may offer significant improvement in tribological properties of the surface of mechanical parts. Under fluid lubrication conditions, the cavitation effect induced by texture can significantly increase the bearing capacity[5, 6] of the friction pair. Therefore, the theoretical and experimental research on the texture induced cavitation effect is very important to improve the lubrication [7–9] of mechanical parts and reduce energy consumption. [10]

Generally, the optimization design works mainly concentrate on three aspects : the geometric parameters, three-dimensional morphology, and texture distribution mode[11, 12]which are the main factors of the hydrodynamic lubrication performance of the surface texture. Siripuram and Stephens [13] conducted a numerical analysis on the texture of pits and protrusions with different morphologies. Through experimental studies, it was found that the friction coefficient depends on the texture size[14]. Moreover, the shape and arrangement direction of the micro-texture have a greater impact on the bearing capacity of the oil film dynamic pressure lubrication. However, in the different contact types and friction conditions, it is difficult to reach a unified conclusion to select the texture parameters. Therefore, when designing textures, more theoretical foundations are needed as guidance.Liu [15] et al. established a two-dimensional model of asymmetric micro-texture, and studied the influence of the outlet inclination angle of the texture on the fluid pressure distribution, flow field, upper wall bearing capacity and friction coefficient in the texture area. It is believed that the triangular texture exit slope will form, and increase a protruding vortex zone, which can enhance the bearing capacity and reducing the coefficient of friction.Jiang et al. [16] used ANSYS Fluent to establish a numerical model of the three-dimensionalflow

field [17] of a mechanical seal with an elliptical texture, and studied its influence mechanism. They believed that the direction of the elliptical texture distribution would affect the pressure distribution of the flow field.

In order to more intuitively study the mechanism of texture-induced cavitation [18, 19], the visualized experimental study of cavitation is particularly important.Reiner Wahl et al. [20] used the pin-disk experiment to observe the cavitation induced by the textured surface of the mesh groove, and found that bubbles exist in the form of small tails at the downstream end of the convex body, or surround the two sides of the convex body. They also found that a certain speed must be reached before cavitation occurs. In summary, that there are fewer simulation and experimental studies on micro-textured arrays, and the study on the influence of micro-textured arrays on the cavitation effect has not been carried out.

The purpose of this study is to explore how the micro-textured array regulates the occurrence of cavitation.Section 2 describes the establishment, solution and analysis of the micro-textured array model. Considering the cavitation effect, three-dimensional numerical simulation of the surface microtexture is carried out by using ANSYS-Fluent software to study the influence of texture distribution modes on the lubrication performance.In order to verify the rationality of the simulation results, the corresponding experiments are carried out by a visual plane sliding platform to analyze the formation of cavitation bubbles. Experimental details, analysis and results are presented in Sections 3 and 4. Finally, the conclusions are provided in the last section.

2 Result

2.1 Simulation of micro-textured arrays

2.1.1 Geometric model

When studying the influence of micro-texture on the fluid lubrication effect, most scholars choose to simulate the flow field of a single texture, but ignore the mutual influence between textures. The cooperation relationship between the texture is not clear yet, which is worthy of further study. Therefore, this study establishes a 4×4 micro-texture array model as shown in Fig. 1 for simulation calculation analysis.

2.1.2 Numerical validation

In this study, the ANSYS-Fluent three-dimensional double-precision solver is adopted for simulation calculation, and *k-ε* turbulence model. The cavitation simulation uses the Mixture multiphase flow model and the Schnerr-Sauer cavitation model. The pressure-velocity coupling uses the Coupled method, the momentum term and energy term are both selected as Quick, the pressure term is in the *PRESTO!* format, and the convergence factor is 1×10^{-5}. In order to facilitate the calculation, the remaining conditions are chosen as Default. The solution process mainly includes the establishment of the geometric model and the meshing, the setting of boundary conditions, physical parameters and the solution method, and the

post-processing analysis with *Tecplot* software. The physical parameters used in the simulation are shown Table 1.

Table 1
Parameters for the numerical experiments

Calculation parameters	Numerical value
Atmospheric reference pressure	101325.1 p_0/Pa
Cavitation pressure	30000 p_c/Pa
Lubricating oil viscosity	0.098η/(Pa·s)
Lubricant density	891ρ/(kg·m^{-3})

In order to compare the effects of different texture models on the lubrication performance, dimensionless bearing capacity, dimensionless friction and friction coefficient *f* are selected to characterize the lubrication performance of the friction pair:

$F_y =$ \iint \overline {{{F_y}}} =\frac{{{F_y}}}{{{F_0}}}=\frac{{{F_y}}}{{{p_0}{S_d}}} (1)

{F_x}=\iint \tau 'dxdz \overline {{{F_x}}} =\frac{{{F_x}}}{{{F_0}}}=\frac{{{F_x}}}{{{p_0}{S_d}}} (2)

f=\frac{{{F_x}}}{{{F_y}}}
3
In the formula, F_y is the normal bearing capacity, *p(x, z)* is the pressure distribution on the upper wall, F_0 is the reference force, p_0 is the atmospheric pressure, F_x is the tangential friction force, and τ' is the shear force.

2.2 Experiment

In the section, in order to verify the occurrence and behavior of cavitation induced by the micro-textured array, the lubrication test and observation of texture samples were carried out on a self-made visual tribo-tester.

2.2.1 Experimental apparatus and Specimen preparation

Figure 2 shows a schematic diagram of the visual flat tribo-testers. The upper sample is tightened by the clamp(9), and the lower sample is connected to the rotating unit which is driven by a stepping motor, and lubricating oil is added between the samples. The vertical load is applied to the support rod by the loading handwheel(6). The loading force is measured by the pressure sensor 7, and the friction force is measured by the pressure sensor 2. A microscope is used to observe through the glass sample (10) from below and to take cavitation image.In this experiment, in order to facilitate preparation and observation,

the upper sample is made of brass; and it is designed into a cylindrical shape with rectangular section of 1.2 mm×2.0 mm to facilitate installation and match with the lower sample.

2.2.2 Experimental procedure

In this experiment, Castrol 5W-40 lubricanting oil is used as lubricant. The kinematic viscosity is 86 mm^2/s (40 ℃) and 13.7 mm^2/s (100 ℃) respectively, and its density at room temperature (25 ℃) is 0.856 g/cm^2. The experiment is carried out at room temperature, the dynamic viscosity of the lubricanting oil at room temperature is 0.0933 *Pa·s*. Before the experiment, sufficient lubricating oil is added in the oil tank of the rotating disc, and the textured sample is immersed into the lubricating oil. The tribo-tester needs to operate under no-load, low speed and sufficient lubrication for a period of time, so that a small amount of air stored in the texture pit can flow out with the lubricating oil. When there are no more bubbles in the texture, stop the rotating unit, reset the test load, speed and other parametersand, and restart the rotating unit for formal test. The final test results are obtained through measuring frictiona and other related parameters under stable conditions, and monitor and photographing the cavitation images of the friction surface in real time through an image acquisition system.

3 Discussion

3.1 Analysis of simulation

3.1.1 The effect of texture arrays of different shapes

Figure 3(a) shows the dimensionless bearing capacity of texture array of different shapes at a speed of 6 m/s, the specimen with parallelogram texture array has the maximum bearing capacity. Figure 4 shows the pressure distribution on the upper wall of the texture array with different shapes. From Figs. 4(a) and (b), it can be concluded that due to the confluence role of textures, the maximum pressure of the convergent trapezoidal texture array is greater than that of the divergent trapezoidal texture array, but the area of the boost zone is much smaller than that of the divergent trapezoidal texture array, which eventually leads to lower total bearing capacity for the sample with convergent trapezoidal texture array.The reason is that for the texture array the mutual influence of adjacent textures perpendicular to the motion direction needs to be considered. Therefore, it can be concluded from Figs. 4(c) and (d), the highest pressure of the diamond array texture is greater than that of the parallelogram, but the high pressure peak area and low pressure cavitation area of the parallelogram have both shifted. So the inhibition between the front and rear microtextures is reduced, and the overall bearing capacity is enhanced, which is better than that of the rhombic texture array, which is the same as the simulation result of single texture.

3.1.2 Influence of Parallelogram Textured Array Distribution Mode

As shown in Fig. 3(b), the dimensionless bearing capacity of five different distribution patterns of micro-textured arrays at speed of 6m/s is compared.From the figure,it can be seen from the figure that the matching mode between the micro-textures has a stronger influence on the flow field and pressure field in the numerical simulation than simply changing the shape of the textures.

Figure 4(e)(f)(g)(h) show the pressure distribution of the square micro-textured array and the three different pattern arrays. Different patterns of parallelogram texture arrays will not only change the pressure field of the fluid domain, but also affect the flow field. From the streamline diagram of the square texture array, it can be seen that the streamlines are only partially bent near the texture entrance and exit, and the adjacent textures will not affect their respective flow fields. In the single-symmetric and pair-symmetric texture arrays, the inclination of the parallelogram texture makes the flow field appear obvious confluence effect, which is conducive to the production of higher oil film pressure. The streamlines in the texture array with single orientation are obviously inclined, but there is no effect of confluence, and the lateral flow of the fluid will cause energy dissipation, weaken the dynamic pressure effect of the texture, and make it the lowest carrying capacity.Similar to the parallelogram texture in the single-texture simulation, the texture arrays of other different distribution patterns also have the effect of reducing the suppression effect between the front and back textures, because the high-pressure peak area and the low-pressure cavitation area have shifted. The high pressure area of the outlet can better extend to the direction of fluid flow.

3.1.3 Influence of the tilt angle of the parallelogram texture array

Figure 5(a) shows the pressure distribution of texture array with single symmetry orientation.As shown in Fig. 5(b), in single symmetry orientation texture array, as the tilt angle increases, the pressure on the center line e of the upper wall increases significantly. With the increase of the inclination angle of the microtexture, the outlet pressurization zone of the second and third rows of microtexture will be closer, which improves the oil film pressure. However, if the inclination angle of the micro-texture is too large, it will reduce the range of the pressurized zone and affect the Oil film pressure.

Figure 5(c) shows the pressure distribution of a multi-symmetrical orientation texture array.As shown in Fig. 5(d), the oil film pressure on the straight line f between the first and second rows of textures will gradually increase as the tilt angle increases. In addition, it can be seen from Fig. 5(e) that the increase in the inclination angle of the textures will reduce the pressure on the center line g of the upper wall surface.

Figure 5(f) shows the pressure distribution on the upper wall of the textured array with a single orientation when the tilt angle is 45°. It can be concluded that texture array with single orientation cannot converge pressure.Take the straight line h at the exit of the third row of textures to analyze the pressure distribution ,as shown in Fig. 5(g). As the tilt angle increases, the pressure peak at the exit of the parallelogram texture shifts to the tilt direction, and the pressure also reduce accordingly at the same time. Therefore, it is believed that parallelogram micro-textured array with single orientation has no effect on improving the

bearing capacity compared to a square texture, and the larger the tilt angle, and the increase of the tilt angle will weaken the dynamic pressure effect of the texture.

3.1.4 Influence of the speed of the upper wall

Figure 6(a) shows the dimensionless bearing capacity of the square texture array and three parallelogram texture arrays with an inclination of 26.6°. With the increase of speed, the dimensionless bearing capacity of all pattern texture arrays gradually increases, and the difference in bearing performance between different pattern arrays is obvious. Within the speed range studied in this paper, the bearing capacity of the single-symmetric orientation texture array is always the best.

Figure 6(b)(c)(d)(e)show the dimensionless bearing capacity of a asymmetrically oriented texture array with different tilt angles under different speed conditions.It can be seen from the figure that under various speed conditions, the asymmetric orientation array has an optimal tilt angle to make the dimensionless bearing capacity the highest. As the speed increases, the optimal tilt angle tends to increase. When the speed is 18 m/s, the optimal tilt angle of the unisymmetric asymmetric array increases from 26.6° to 36.9°. This is because the increase in speed will increase the suppression of the dynamic pressure effect between the front and rear textures, and the greater the inclination angle of the parallelogram, the more conducive to staggering the low pressure zone at the entrance of the texture and the high pressure peak zone at the exit in the flow direction. The high-pressure zone of the texture outlet extends backward in the direction of flow, thereby increasing the range of the high-pressure zone.

3.2 Analysis of experiments results

3.2.5 Experiments on micro-textured arrays of different shapes

The fixed load is 10 N, and the experiment is carried out under different speed conditions to compare the friction coefficient of the non-textured sample and five kinds of texture samples of different shapes.the five texture arrays of different shapes can improve the lubricating performance of the friction pair compared with the non-textured samples, and their friction coefficients are all reduced.

When the speed is 6 r/min (0.019 m/s), the friction coefficient of samples are not much different. When the speed is low, the oil film of the friction pair has not been fully formed, and the texture has little effect on the improvement of the oil film bearing capacity. When the speed is greater than 18 r/min (0.057 m/s), the lubricating performance of the sample with the convergent trapezoidal texture is always the smallest. When the speed is 24 r/min(0.076 m/s), the cavitation pictures of texture arrays with different shapes are shown in Fig. 7. It can be inferred from the Figure that cavitation has occurred on the surface of the textured samples of various shapes. However, the different texture distribution positions will cause the pressure distribution around the texture to be different, and the cavitation bubbles caused by the texture will also be significantly different. The textures located downstream of the texture array are more prone to drag out cavitation bubbles. The reason is that these textures are closer to the pressure outlet and the

surrounding oil film pressure is relatively low. In addition, comparing the cavitation bubbles induced by texture arrays of different shapes, it can be seen that the convergent trapezoidal texture array produces the least bubbles, while the divergent trapezoid texture induces the most cavitation bubbles.

3.2.6 Experiments on micro-textured arrays with different distribution patterns

Figure 7 shows the cavitation state of three different parallelogram texture array samples at speed of 24 r/min. It can be seen from the figure that only a small part of the textures in asymmetric orientation texture array hascavitation bubbles overflowing. In texture array with multiple symmetrical orientations, there are certain cavitation bubbles at the rear end of the outlet. The cavitation effect induced by the single orientation texture array is the most severe, which is due to the convergence of the cavitation bubbles of the upstream and downstream textures, forming a larger cavitation area. Comparing the pressure distribution of the texture array with different modes in the previous simulation, it can be seen that the area where the oil film pressure is higher is less likely to form cavitation bubbles.

3.2.7 Experiment on the oil film thickness of different pattern micro-textured arrays

In order to further analyze the mechanism of the improvement of tribological performance by texture arrays of different patterns, the laser displacement sensor is used to estimate the oil film thickness. It can be seen from Fig. 8 that compared with the non-textured sample, the oil film thickness of other texture modes all have increased. Combining the previous simulation analysis, combined with the previous simulation analysis, it is found that the oil film bearing capacity of the textured array is directly proportional to the oil film thickness. This conclusion is consistent with the literature [35]. The increase of the oil film thickness will reduce the friction coefficient of the sample and enhance the lubricating performance. Thus, the increase in the thickness of the oil film means that the direct contact area of the upper and lower sample is reduced, which makes the lubrication more sufficient.

4 Conclusions

On the basis of the calculations and experiments, conclusions are drawn as follows:

1. Cavitation is one of the main reasons for microstructure to improve the bearing capacity of oil film.

2. The micro-textured array simulation results show that, the single-symmetric orientation texture array is most conducive to the improvement of oil film bearing capacity, and the bearing effect is the best when the texture inclination is 26.6°. The interaction between the textures can significantly change the pressure distribution and flow field of the fluid distribution domain.
3. Experimental results show that surface textures can improve the lubrication effect of the friction pair, mainly because the micro-textured array improves the bearing capacity of the oil film and increases the thickness of the oil film.

4. The friction coefficient of the asymmetrically oriented textured sample is 29.4% lower than that of the untexture sample, and the lubrication performance is the best.

Declarations

Acknowledgements

This paper is based on the research work supported by the National Nature Science Foundation of China (NSFC) (No. 51779023).

Author contributions

YY.J, ZJ. Y and SW.z. contributed to the design and implementation of the research, to the analysis of the results and to the writing of the manuscript.

Competing interests

The authors declare no competing interests.

References

1. Yu H, Wang X, Zhou F. Geometric Shape Effects of Surface Texture on the Generation of Hydrodynamic Pressure Between Conformal Contacting Surfaces[J]. Tribology Letters **37**(2):123–130(2010)
2. Woloszynski T, Podsiadlo P, Stachowiak G W. Efficient Solution to the Cavitation Problem in Hydrodynamic Lubrication[J]. Tribology Letters **58**(1):18(2015)
3. Yang, Mao, Liangcai, et al. Modeling and optimization of cavitation on a textured cylinder surface coupled with the wedge effect[J]. Tribology International **104**(12):212–224(2016)
4. Shi X, Ni T. Effects of groove textures on fully lubricated sliding with cavitation[J]. Tribology International **44**:2022–2028(2011)
5. Etsion I. Improving Tribological Performance of Mechanical Components by Laser Surface Texturing[J]. Tribology Letters **17**(4):733–737(2004)
6. Gropper D, Wang L, Harvey T J. Hydrodynamic lubrication of textured surfaces: A review of modeling techniques and key findings[J]. Tribology International **94**:509–529(2016)
7. Hamilton D B, Walowit J A, Allen C M. A theory of lubri-cation by microirregularities. J Basic Eng **88**(1): 177–185 (1966)
8. Brizmer V, Kligerman Y, Etsion I. A laser surface textured parallel thrust bearing. Tribol Trans **46**(3): 397–403 (2003)
9. Wang X L, Kato K, Adachi K, Aizawa K. Loads carrying capacity map for the surface texture design of SiC thrust bearing sliding in water. Tribol Int **36**(3): 189–197 (2003)

10. Putignano C, Scarati D, Gaudiuso C, et al. Soft matter laser micro-texturing for friction reduction: An experimental investigation[J]. Tribology International **136**:82–86(2019)
11. Wang X, Adachi K, Otsuka K, Kato, K. Optimization of the surface texture for silicon carbide sliding in water. Applied Surface Science **253**(3):1282–1286(2006)
12. Liu D, Yan Z, Yan X, et al. The simulation of asymmetric micro-textures on the lubrication characteristics of sliding friction pairs. IOP Conference Series: Earth and Environmental Science **240**(6).(2019)
13. Siripuram R, Stephens L S. Effect of Deterministic Asperity Geometry on Hydrodynamic Lubrication[J]. Journal of Tribology **126**:527–534(2004)
14. Gropper D, Wang L, Harvey T J. Hydrodynamic lubrication of textured surfaces: A review of modeling techniques and key findings. Tribol Int **94**: 509–529 (2016)
15. Liu D, Yan Z, Yan X, et al. The simulation of asymmetric micro-textures on the lubrication characteristics of sliding friction pairs[J]. IOP Conference Series: Earth and Environmental Science **240**(6):062019–062030(2019)
16. Jiang S, Ji H, Wang T, et al. Enhanced understanding of leakage in mechanical seals with elliptical dimples based on CFD simulation[J]. Industrial Lubrication and Tribology **72**(1):24–30(2020)
17. Brajdicmitidieri P, Gosman A D, Ioannides E, et al. CFD Analysis of a Low Friction Pocketed Pad Bearing[J]. Journal of Tribology-transactions of The Asme 127(4): 803–812(2005)
18. Profito F J, Vlădescu S, Reddyhoff T, et al. Transient experimental and modelling studies of laser-textured micro-grooved surfaces with a focus on piston-ring cylinder liner contacts[J]. Tribology International **113**:125–136(2017)
19. Wang T, Huang W, Liu X, et al. Experimental study of two-phase mechanical face Seals with laser surface texturing[J]. Tribology International **72**:90–97(2014)
20. Wahl R, Schneider J, Gumbsch P. In situ observation of cavitation in crossed microchannels[J]. Tribology International **55**(2):81–86(2012)
21. Wang W, He Y, Zhao J, et al. Optimization of groove texture profile to improve hydrodynamic lubrication performance: Theory and experiments[J]. Friction 8(01):83–94(2020)

Figures

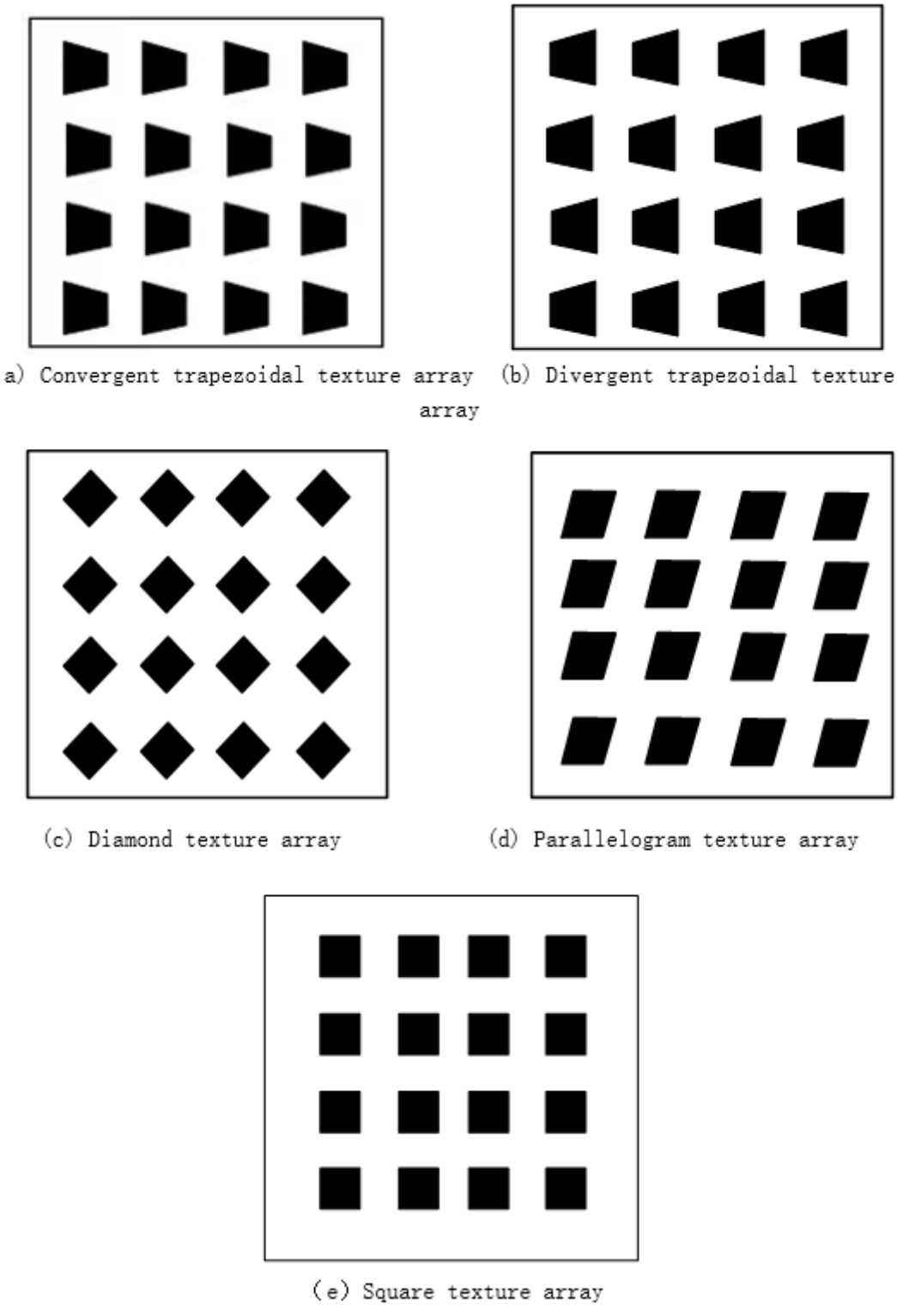

Figure 1

Five types of 4×4 microtexture array layout

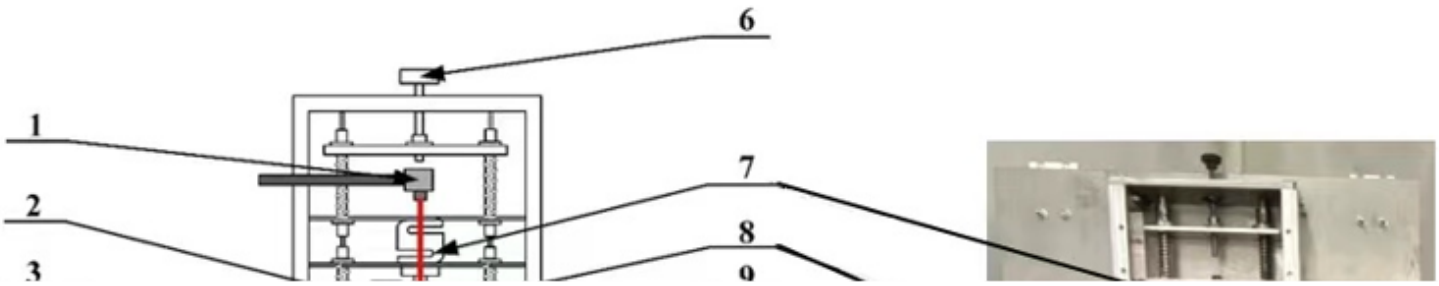

Figure 2

Sample and Fixture Assembly Drawing

1. Laser distance meter 2. Friction sensor 3. Upper sample 4. Lubricating oil 5. Microscope

6. Loading handwheel7. Loading force sensor 8. Support rod 9. Upper sample holder

10. Lower sample 11. Rotary table

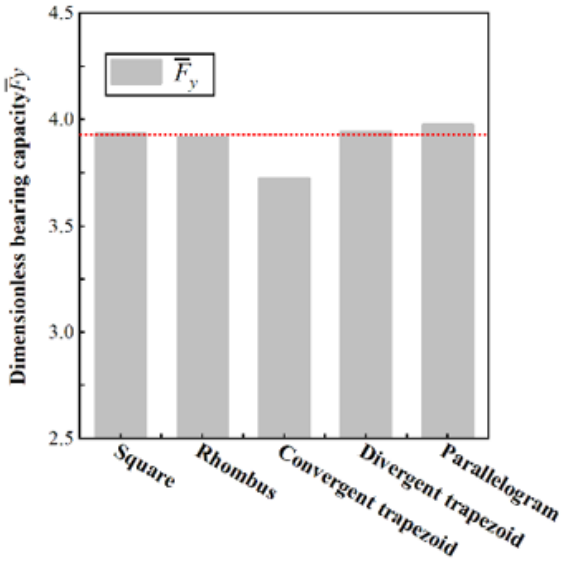

(a) Dimensionless bearing capacities of texture arrays of different shapes

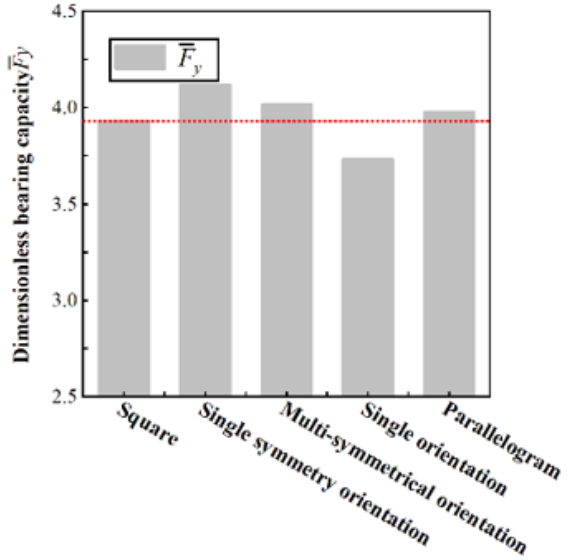

(b) Dimensionless bearing capacities of microtexture arrays of different modes

Figure 3

Dimensionless bearing capacities

Figure 4

Pressure distribution

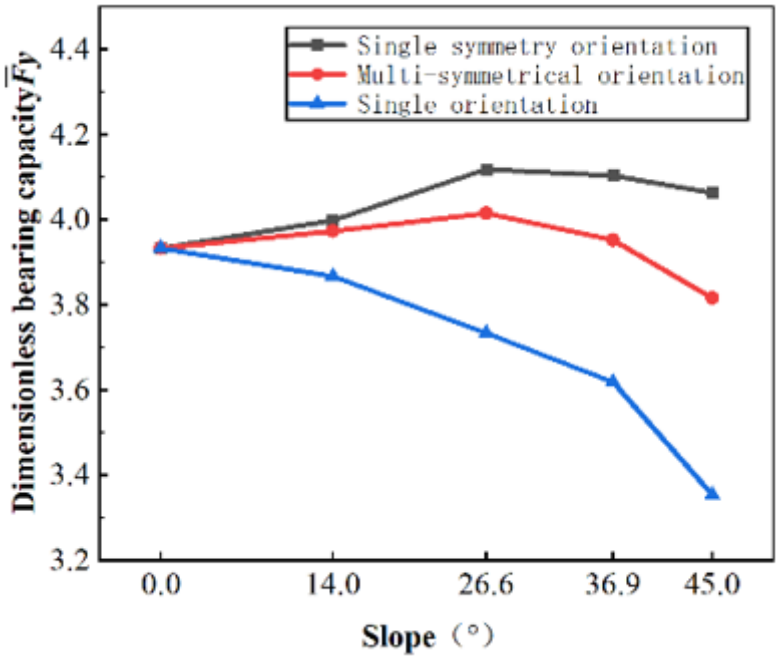

Figure 5

Dimensionless bearing capacity at different inclination angles

Figure 6

Pressure distribution with different tilt angles

(a) The pressure distribution of the texture array with a tilt angle of 45°

(b) Pressure distribution on the center line of the upper wall

(c) The pressure distribution of the texture array with a tilt angle of 45°

(d) Pressure distribution on the upper wall line f

(e) Pressure distribution on the upper wall center line g

(f) The pressure distribution of the texture array with a tilt angle of 45°

(g) Pressure distribution on the upper wall line h

Figure 7

bearing capacity

Figure 8

Cavitation images

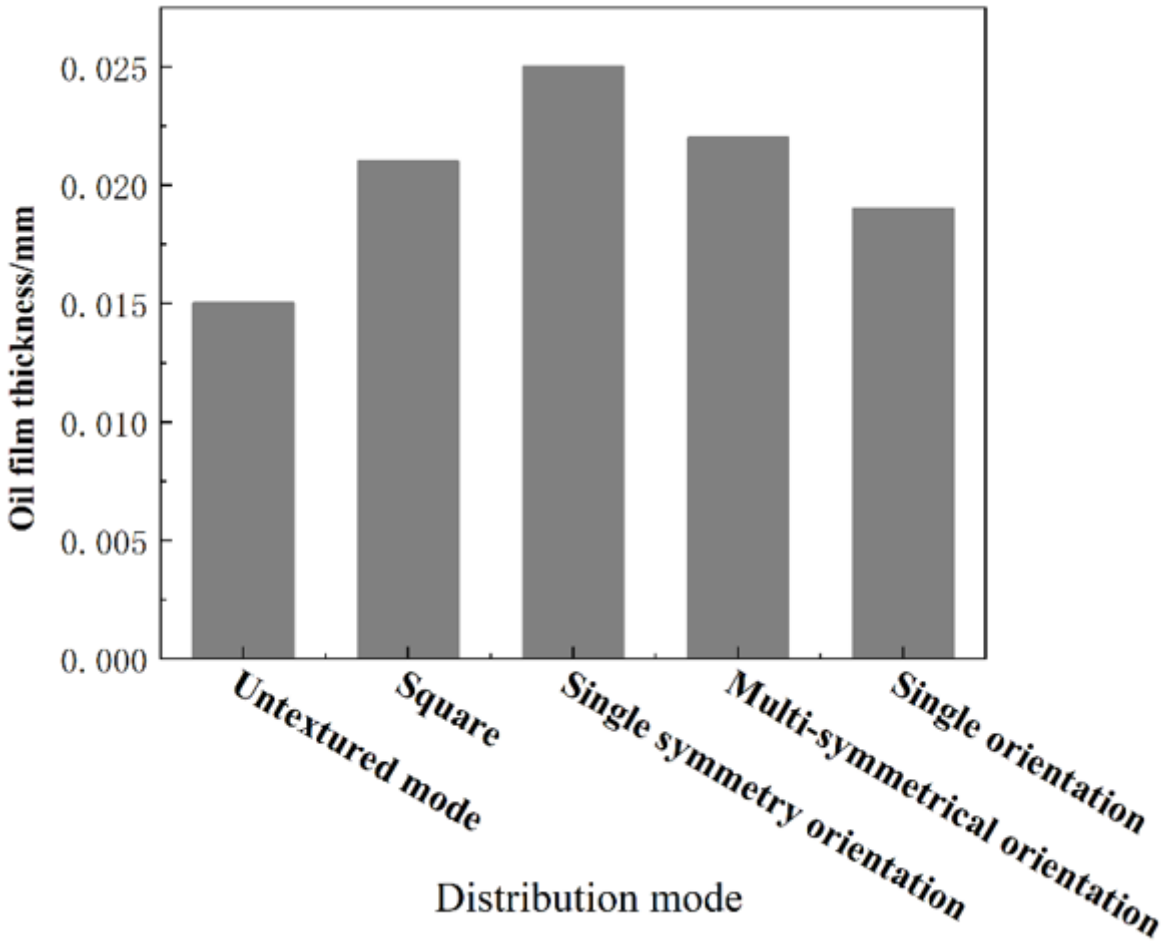

Figure 9

Oil film thickness of texture array with different patterns